Journal of Applied Physics ARTICLE pubs.aip.org/aip/jap

Self-activated growth of cubic AlScN films from molecular nitrogen without plasma

Cite as: J. Appl. Phys. **139**, 075307 (2026); doi: 10.1063/5.0322931
Submitted: 14 January 2026 · Accepted: 16 January 2026 ·
Published Online: 20 February 2026

View Online Export Citation CrossMark

Chandrashekhar Savant,[1,a)] Rishabh Singh,[2] Thai-Son Nguyen,[1] Joseph Casamento,[3] Huili Grace Xing,[1,4,5] and Debdeep Jena[1,4,5,a)]

AFFILIATIONS

[1]Department of Materials Science and Engineering, Cornell University, Ithaca, New York 14853, USA
[2]Department of Applied and Engineering Physics, Cornell University, Ithaca, New York 14853, USA
[3]Department of Materials Science and Engineering, Massachusetts Institute of Technology, Cambridge, Massachusetts 02142, USA
[4]School of Electrical and Computer Engineering, Cornell University, Ithaca, New York 14853, USA
[5]Kavli Institute at Cornell for Nanoscale Science, Cornell University, Ithaca, New York 14853, USA

Note: This paper is part of the Special Topic on Frontiers in Nitride Semiconductors Research.
[a)]**Author to whom correspondence should be addressed:** cps259@cornell.edu and djena@cornell.edu

ABSTRACT

Self-activated growth of ScN was recently reported owing to the ability of scandium to self-catalyze N_2 bond breaking, facilitating nitride film growth from molecular N_2 without plasma. In this report, we expand this novel synthesis method to explore the possibility of self-activated growth of aluminum–scandium–nitride, an emerging ternary nitride system with enhanced functionalities. We find that the *rock salt* AlScN film growth of low Al composition from 0% to 48% is possible by self-activated growth. The cubic rock salt AlScN films are phase pure up to 21% Al, whereas mixed rock salt AlScN and intermetallic cubic Al_xSc phases appear in films with 28% to 48% Al. Self-activated nitride crystal growth was not observed for films grown with high Al content of 93.7% and 100% Al, which showed cubic Al_xSc and FCC α-Al phases, respectively, without any sign of nitrogen incorporation. Lattice parameters of crystalline rock salt AlScN films decrease with increasing Al composition. The self-activated AlScN films, as well as cubic Al_xSc and FCC α-Al phase, exhibit twinning and are epitaxial to the 6H-SiC substrate. The findings open up new avenues for the ultralow-energy synthesis of ternary nitrides and beyond.

I. INTRODUCTION

Group III-A nitride semiconductors, such as AlN, GaN, and InN, and their alloys have revolutionized solid-state lighting, acoustic devices, and high-power electronics in recent decades.[1–4] Transition metal nitrides are also of tremendous technological significance due to their mechanical, thermal, magnetic, metallic, and superconducting properties.[1] Alloying of group III-A nitride with transition metals further enhances their properties and imparts new functionalities.[1,5–8] For instance, ternary alloys of transition metal and group III-A metal nitrides such as TiAlN, CrAlN exhibit excellent wear and high-temperature oxidation resistance and are well-known as protective coating materials.[5,9–11] Adding isovalent group III-B Sc to GaN, AlN, InN electronics and photonics family introduces new properties that were previously absent, including thermoelectric,[12,13] plasmonic,[14] lattice matching,[15–17] extraordinarily high piezoelectric,[18] ferroelectric,[19–21] and high dielectric constant[22–24] characteristics.

Traditional non-ammonia based inorganic synthesis of these nitrides from N_2 gas mainly relies on energetic plasma to break the dinitrogen N≡N triple bonds that have a bond strength of 9.8 eV/molecule.[25] Scandium, a group III-B transition metal, has recently been reported to have a strong scavenging effect on gettering/capturing gas species.[26] Utilizing the ability of scandium to self-catalyze N_2 bond breaking, it was found that binary ScN films could be epitaxially grown from molecular N_2 without plasma over a wide range of temperatures.[26] Earlier studies have also

demonstrated that Sc can react with and activate molecular N_2 under plasma-free conditions, including nitridation of Sc metal with N_2 gas,[27,28] molecular N_2 cleavage by Sc–Sc species forming Sc_4N_4 clusters,[29] thin-film ScN growth directly from molecular N_2 at elevated temperatures,[30] and catalytic effect of Sc during N_2 plasma-assisted AlScN and ScGaN growth.[30–32] Can ternary Al–Sc nitride films be grown without plasma as well?

This report evaluates the feasibility of plasma-free self-activated growth of AlScN films from molecular N_2 at varying aluminum compositions. The phase, crystal structure, and epitaxial registry of the $Al_xSc_{1-x}N_y$ films grown on the (0001) 6H-SiC substrate are measured. The Al composition is varied from 0% to 100% ($x = 0$–1) to determine various crystal phases formed. The structural lattice parameters of self-activated cubic rock salt AlScN films, cubic Al_xSc, and FCC α-Al are reported in this work. The range of Al compositions where the self-activated growth of ternary Al–Sc nitride films is feasible is determined.

II. EXPERIMENTAL

All growths in this study were performed using a Veeco GenXplor molecular beam epitaxy (MBE) system with an idle base pressure of 5×10^{-10} Torr. A solid scandium source of 99.9% purity on a rare earth element basis obtained from Ames Laboratory was loaded in a tungsten crucible and evaporated using an effusion cell. An aluminum source of 99.9999% purity obtained from United Mineral & Chemical Corp. (UMC) was loaded into a pyrolytic boron nitride (PBN) crucible and evaporated using an effusion cell. A 99.999 95% purity N_2 gas was supplied without striking plasma during all growths in this study. A kSA Instruments reflection high-energy electron diffraction (RHEED) apparatus with a Staib electron gun operating at 14.5 kV and 1.45 A was used to monitor the film growth. The RHEED diffraction images were acquired along the [11$\bar{2}$0] zone axes of the 6H-SiC substrates during the MBE growth.

The $Al_xSc_{1-x}N_y$ films in this study were grown on [0001] oriented Si-face 6H-SiC substrates to assess the reactivity of Sc and Al with molecular nitrogen. Before growth, the SiC substrates were solvent cleaned by sonication for 10 min each in acetone, methanol, and isopropyl alcohol (IPA). Thereafter, the substrates were outgassed at 200 °C, 1×10^{-7} Torr for 8 h and were then in situ transferred to the growth module without a vacuum break. The feasibility of self-activated growth of $Al_xSc_{1-x}N_y$ films over the entire Al composition range from 0% to 100% was assessed by varying the Al/(Al+Sc) flux ratio from 0 to 1 while keeping the total Al+Sc flux at $\sim 2.4 \times 10^{-8}$ Torr. All growths were performed using a nitrogen gas flow rate of 1.8 SCCM and the growth chamber pressure of approximately 4.4×10^{-5} Torr. $Al_xSc_{1-x}N_y$ films of ~135–210 nm thickness were grown at a substrate thermocouple temperature of 550 °C. The actual substrate temperature, as calibrated by Ga droplet desorption test,[33] is about 50 °C higher than the reported substrate thermocouple temperature of 550 °C, with details provided in our earlier work.[34]

X-ray diffraction (XRD) $2\theta - \omega$ spectra were collected using a Panalytical Empyrean diffractometer with a 1.5406 Å Cu Kα x-ray source operated at 45 kV, 40 mA to characterize the phase, crystal structure, and orientation of the $Al_xSc_{1-x}N_y$ films. The compositions of the grown $Al_xSc_{1-x}N_y$ films were analyzed with energy-dispersive x-ray spectroscopy (EDS/ EDAX) using a Zeiss Supra SEM (scanning electron microscope) operated at 20 keV and using a Bruker energy dispersive x-ray spectroscopy (EDS) silicon drift detector (SDD). Characteristic x-ray energy peaks corresponding to N Kα (0.3924 keV), Al Kα (1.486 keV), and Sc Kα (4.091 keV)[35] were used to determine $Al_xSc_{1-x}N_y$ film composition, with Al composition expressed as x = [Al]/([Al]+[Sc]) ratio and N composition expressed as y = [N]/([Al]+[Sc]) ratio.

III. RESULTS AND DISCUSSION

Figure 1(a) shows the schematic of $Al_xSc_{1-x}N_y$ films grown on a 6H-SiC substrate in this study from molecular N_2 without striking plasma. Figures 1(b)–1(f) show the *in situ* reflection high-energy electron diffraction (RHEED) patterns of $Al_xSc_{1-x}N_y$ films grown with increasing Al/(Al+Sc) composition from 0% to 100%. Figure 1(b) shows the RHEED diffraction pattern of a self-activated twin-cubic rock salt ScN film, i.e., the 0% Al-containing stoichiometric ScN film grown using an Al/(Al+Sc) flux ratio, $x = 0$%. A similar self-activated growth of ScN film was recently reported using molecular nitrogen without plasma, owing to the strong scavenging effect of Sc on gettering residual gas species in the

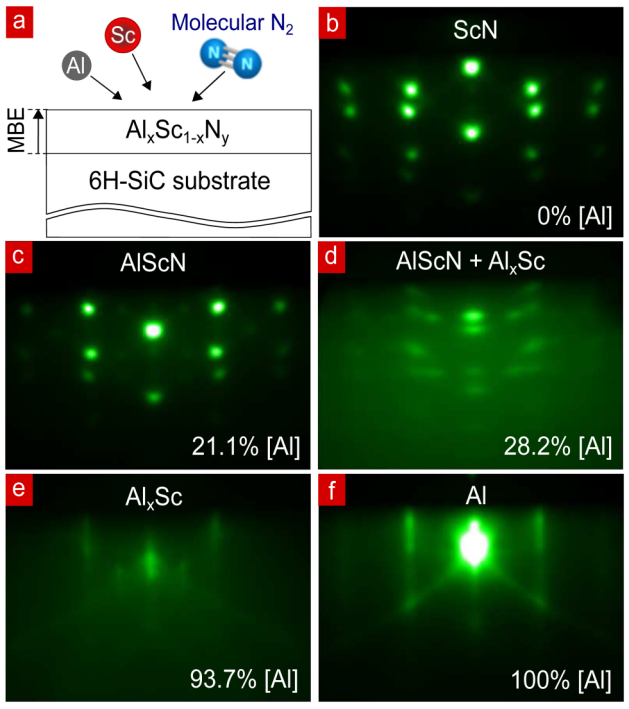

FIG. 1. (a) Heterostructure schematic of the self-activated $Al_xSc_{1-x}N_y$ films grown from molecular N_2 on the [0001] oriented Si-face 6H-SiC substrate at 550 °C and reflection high-energy electron diffraction (RHEED) patterns collected at 550 °C substrate temperature for (b) twin-cubic rock salt ScN film with 0% Al (c) twin-cubic rock salt AlScN film with 21.1% Al (d) mixed twin-cubic rock salt AlScN + intermetallic Al_xSc film with 28.2% Al, (e) intermetallic Al_xSc film with 93.7% Al, and (f) face-centered cubic (FCC) aluminum film with 100% Al.

chamber.[26] *Ab initio* calculations identified a possible energetic pathway for the self-activated growth of crystalline ScN films from molecular nitrogen.[26]

Al content in the self-activated $Al_xSc_{1-x}N_y$ films was increased by increasing the Al/(Al+Sc) flux ratio. Figure 1(c) shows the RHEED diffraction pattern of self-activated $Al_xSc_{1-x}N_y$ film with 21.1% Al. The self-activated AlScN films grown without plasma with compositions from 0% Al to 21.1% Al show a similar RHEED diffraction pattern (Figs. S1 and S2 in the supplementary material) corresponding to twin-cubic rock salt AlScN films. No additional diffraction spots were observed in the films grown with 0%–21.1% Al, suggesting phase-pure twin-cubic rock salt AlScN films. The RHEED diffraction patterns in Figs. 1(b) and 1(c) (Figs. S1 and S2 in the supplementary material) signify self-activated epitaxial growth of [111] oriented twin-cubic rock salt AlScN films on an [0001] oriented 6H-SiC substrate. These diffraction patterns indicate 60° rotated domains with two separate overlaid $[1\bar{1}0]$ zone axes, with pairs of {111} and {002} families of planes as indexed in Fig. S1 in the supplementary material.[26]

For the films containing 28.2% to 47.8% Al, RHEED diffraction spots corresponding to an intermetallic Al_xSc phase appear in addition to the twin cubic rock salt AlScN phase. This indicates that the self-activated films grown between 28.2% Al and 47.8% Al have mixed twin-cubic rock salt AlScN and intermetallic Al_xSc phases. Due to the thermodynamic stability of the cubic rock salt structure of AlScN for compositions from 0% to ∼ 47.8% Al, (111) oriented rock salt AlScN phase forms instead of wurtzite or zinc blende phases of AlScN.[36–38] Figure 1(e) shows the RHEED diffraction pattern for the film with ∼ 93.7% Al wherein only the intermetallic Al_xSc phase was observed. The diffraction spots corresponding to twin-cubic rock salt AlScN were absent. Figure 1(f) shows a streaky RHEED pattern for 100% Al-containing film sample corresponding to the FCC α-Al film.[39]

The RHEED diffraction patterns shown in Fig. 1 and Figs S1 and S2 in the supplementary material are measured/captured at a 0° ϕ rotation of the sample corresponding to the $[11\bar{2}0]$ zone axis of the 6H-SiC substrate and $[01\bar{1}]$ zone axis of grown cubic phases.[26,40,41] This suggests that the twin-cubic phases grow with their in-plane $[01\bar{1}]$ and $[2\bar{1}\bar{1}]$ directions ∥ $[11\bar{2}0]$ and $[10\bar{1}0]$ directions, respectively, of the 6H-SiC substrate and their out-of-plane [111] direction ∥ [0001] direction of the 6H-SiC substrate. The RHEED diffraction patterns observed for all the films grown in this study repeat at ±60°, 120°, 180° ϕ rotations, suggesting a sixfold symmetry of the twin-cubic rock salt AlScN, intermetallic Al_xSc, and FCC α-Al phases observed. Twin domains of the cubic phase are expected as a result of symmetry constraints imposed upon growing a threefold symmetric cubic crystal on a sixfold symmetric hexagonal substrate.[26,40]

Figure 2 shows the x-ray diffraction (XRD) $2\theta - \omega$ spectra collected for $Al_xSc_{1-x}N_y$ films grown in this study with increasing Al composition from bottom to the top curves. All films showed XRD peaks corresponding to 006 Bragg reflection of the 6H-SiC substrate. For films with 0% to 21.1% Al, only 111 (and 222) Bragg reflections from cubic rock salt AlScN and the 6H-SiC substrate were observed,[38,42] with the AlScN 111 Bragg peak shifting from 34.42° to 36.66° in 2θ as Al content is increased.

At higher Al concentrations from 28.2% to 47.8%, additional x-ray diffraction peaks corresponding to 111 Bragg reflections from cubic intermetallic Al_xSc appear at ∼37.5° to 38° 2θ in addition to cubic rock salt AlScN 111 Bragg reflections.[43] This suggests that the films grown with Al concentrations from 0% to 21.1% Al composition are phase-pure cubic rock salt AlScN. In contrast, the films grown with Al compositions from 28.2% to 47.8% Al composition have mixed phases of cubic rock salt AlScN and cubic intermetallic Al_xSc. This further validates the single-phase RHEED diffraction patterns observed for the films with 0% to 21.1% Al and mixed-

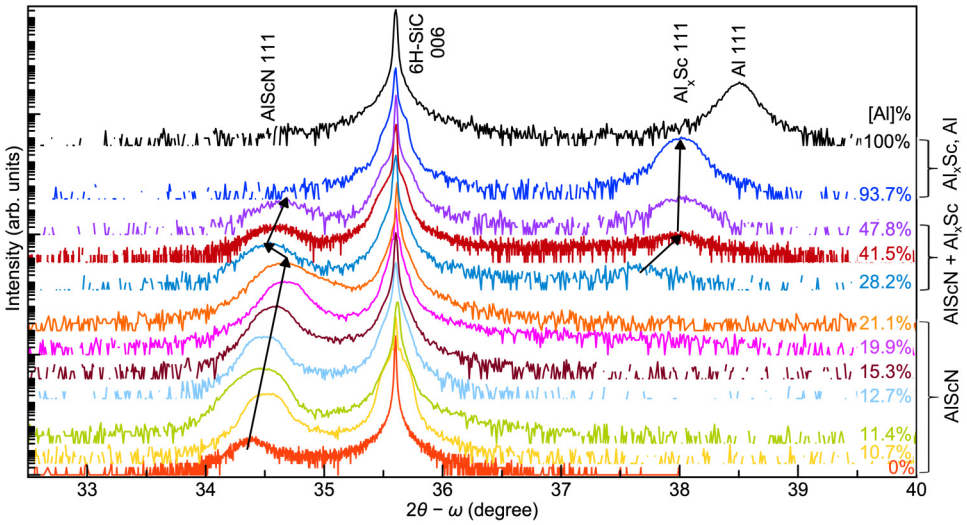

FIG. 2. XRD symmetric $2\theta - \omega$ scans of $Al_xSc_{1-x}N_y$ films with increasing Al composition from 0% Al at bottom curve to 100% Al at top curve. Films with 0% to 21.1% Al show 111 rock salt AlScN and 006 SiC-6H Bragg reflections, indicating the epitaxial growth of phase-pure (111) rock salt AlScN films on the (0001) SiC-6H substrate. An additional peak corresponding to 111 Al_xSc Bragg reflections appears for films with 28.2%–47.8% Al, indicating mixed-phase growth of rock salt AlScN and intermetallic Al_xSc phases. The films with 93.7% and 100% Al have Bragg reflections corresponding to Al_xSc and α-Al, respectively, without any signs of rock salt AlScN peaks. The arrows mark the shift in $2\theta - \omega$ positions of 111 rock salt AlScN and 111 Al_xSc Bragg reflections, indicating a change in lattice parameters of rock salt AlScN and 111 Al_xSc with increasing Al composition.

phase RHEED diffraction patterns observed for the films with 28.2% to 47.8% Al. Cubic rock salt AlScN and intermetallic Al_xSc both grow with their ⟨111⟩ direction parallel to the ⟨0001⟩ direction of the 6H-SiC substrate. The relative ratios of 111 Bragg reflection peaks for intermetallic Al_xSc to that of rock salt AlScN increases with increasing Al content from 28.2% Al to 93.7%, suggesting an increase in the amount of intermetallic Al_xSc phase separation.

For the films with 93.7% Al and 100% Al the Bragg reflections corresponding to rock salt AlScN were not observed in XRD spectra shown in Fig. 2. The film with 93.7% Al exhibits 111 (and 222) Bragg reflections corresponding to intermetallic Al_xSc, confirming Al_xSc growth as observed in RHEED. Bragg reflection corresponding to 111 face-centered cubic (FCC) α-Al metal was observed at 2θ ~38.53° for the film grown with only Al flux (without Sc). Cubic intermetallic Al_xSc and FCC α-Al films also grow with their ⟨111⟩ crystallographic axis along the 6H-SiC ⟨0001⟩ axis.

The shift in $2\theta - \omega$ positions of 111 AlScN and 111 Al_xSc Bragg reflections marked by arrows in Fig. 2 indicates the change in lattice parameter with Al composition. The lattice parameters for the cubic rock salt AlScN extracted from 111 and 222 Bragg reflections are plotted in Fig. 3 in red circles. The self-activated cubic rock salt ScN film (i.e., 0% Al-containing film) has a lattice parameter of 4.504 Å, comparable to the reported values of 4.50–4.51 Å.[13,26,40,44–46] With increasing Al composition from 0% to 21.1%, the lattice parameter of cubic rock salt AlScN film decreases from 4.504 Å for 0% Al to 4.476 Å for 21.1% Al composition. This is expected considering the smaller lattice parameter of cubic rock salt AlN ~4.060–4.085 Å compared to that of ScN ~4.50–4.51 Å.[13,26,38,42,44–46] The shift in 111 AlScN Bragg reflection peaks and decrease in lattice constants of rock salt AlScN films thus confirm the incorporation of aluminum in nitrided form into the AlScN ternary nitride films.[42]

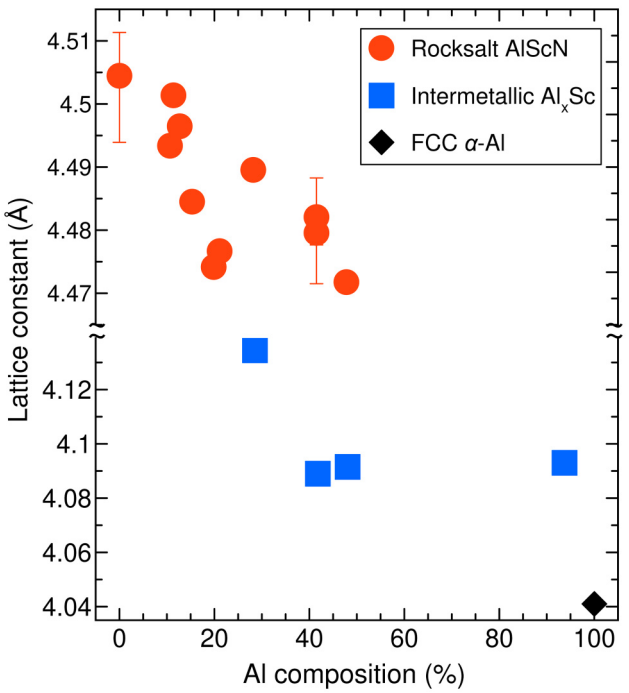

FIG. 3. Lattice constants of cubic rock salt AlScN (red circles), intermetallic Al_xSc (blue squares), and FCC α-Al (black diamond) phases as a function of Al compositions from 0% to 100%. With increasing Al content, the lattice constants of cubic rock salt AlScN, and Al_xSc decrease. An increase in the lattice constant of cubic rock salt AlScN with increasing Al composition from 21.1% to 28.2% coincides with the emergence of the intermetallic Al_xSc phase.

An increase in the lattice parameter of cubic rock salt AlScN from 4.476 Å for 21.1% Al to 4.900 Å for 28.2% Al could be due to the intermetallic Al_xSc phase separation from the cubic rock salt AlScN films, as evident in RHEED and XRD diffraction. The films with a net 28.8% Al composition could have Al-rich intermetallic Al_xSc phase and Al-deficient rock salt AlScN phase with a lower lattice constant. Furthermore, increasing the Al composition from 28.2% Al to 47.8% Al again decreases the lattice parameter of the rock salt AlScN phase from 4.900 to 4.471 Å, likely due to increasing Al content in the rock salt AlScN phase. The lattice parameters for the cubic intermetallic Al_xSc extracted from 111 Bragg reflections are plotted in Fig. 3 in blue squares. With increasing Al composition from 28.2% to 93.7%, the intermetallic Al_xSc Bragg reflection peaks also shift to higher 2θ values from 37.576° for 28.2% Al to 38.021° for 93.7% Al, corresponding to a decrease in lattice constant from 4.136 to 4.093 Å. As marked by the black diamond in Fig. 3, the lattice parameter of metallic FCC α-Al measured from 111 and 222 Bragg reflections for the 100% Al-containing film is 4.040 Å, comparable to reported values of ~4.049 Å.[47]

The Al_xSc phase could have a definite $L1_2$ ordering of Sc atoms in the FCC Al lattice or be a random substitutional solid solution of Sc atoms in the FCC Al lattice.[43] It should be noted that the calculated lattice parameters of Al_xSc phases with $L1_2$ ordering of Sc atoms in FCC Al lattice varies from 4.040 Å for 100% Al to 4.070 Å for 92.6% Al (i.e., $Al_{100}Sc_8$) to 4.101 Å for 75% Al (i.e., Al_3Sc) and the lattice parameters for Sc-substitutional solid solution in FCC Al lattice linearly increases from 4.040 Å for 0% Al to ~4.085 Å for ~93.7% Al to 4.178 Å for 75% Al.[43] The measured lattice parameter of 4.093 Å for ~93.7% Al-containing Al_xSc film is comparable to the calculated lattice parameter of ~4.085 Å for Sc-substitutional solid solution with ~93.7% Al than the lattice parameter of 4.070 Å for $L1_2$ ordered structure (i.e., $Al_{100}Sc_8$).[43] This suggests that the film grown with 93.7% Al is likely a Sc-substitutional solid solution with FCC Al lattice.

The chemical composition of the $Al_xSc_{1-x}N_y$ films grown in this study was measured by EDAX. The EDAX N $K\alpha$ characteristics x-ray spectra in Fig. 4(a) confirm the presence of nitrogen in the $Al_xSc_{1-x}N_y$ films with Al compositions of $x = 0\%$–47.8%. Figure 4(b) shows the [N]/([Al]+[Sc]) ratio plotted as a function of Al composition in the $Al_xSc_{1-x}N_y$ films. A comparable [N]/([Al]+[Sc]) ratio of ~1 to 1.2 is observed for the phase-pure $Al_xSc_{1-x}N_y$ films samples with 0%–21.1% Al. With increasing Al composition, the [N]/([Al]+[Sc]) ratio decreases from 1.04 for 28.2% Al to 0.44, 0.50 for 41.5%, 47.8% Al-containing films and to 0 for 93.7% and 100% Al-containing $Al_xSc_{1-x}N_y$ films. N $K\alpha$ characteristics x-ray peak was not evident in the $Al_xSc_{1-x}N_y$ film samples with

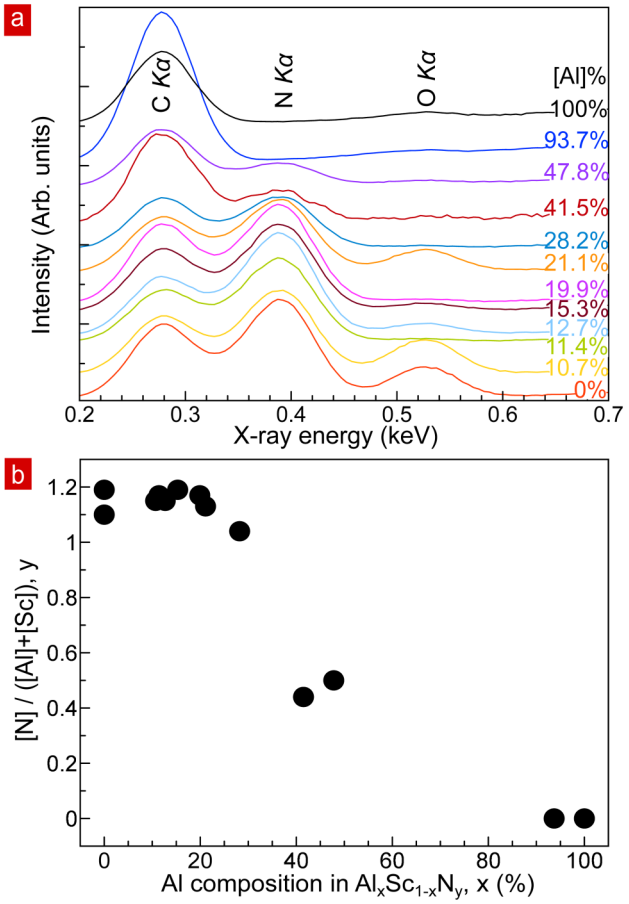

FIG. 4. (a) EDAX C $K\alpha$, N $K\alpha$, and O $K\alpha$ characteristics x-ray spectra, and (b) N composition, expressed as y = [N]/([Al]+[Sc]) ratio for $Al_xSc_{1-x}N_y$ film samples with different Al compositions grown without plasma. The presence of N is evident in the films with 0%–47.8% Al, confirming the self-activated growth of AlScN from molecular N_2. The [N]/([Al]+[Sc]) ratio of films with 0%–21.1% Al is 1–1.2, and it decreases with increasing Al composition of the films.

>93.7 Al, i.e., [N]/([Al]+[Sc]) ratio was 0, suggesting that the self-activated growth of cubic rock salt AlScN was only feasible at high Sc and low Al compositions. AFM micrographs taken over $2 \times 2\,\mu m^2$ area shown in Fig. S3 in the supplementary material, suggest a Volmer–Weber (3D) growth mode for the self-activated AlScN films with 0%–100% Al composition.

Scandium, a group III-B element, exhibits a strong scavenging effect on gettering/capturing residual gas species in the growth chamber; thus, self-activated growth of ScN films is feasible as Sc facilitates N_2 bond breaking and incorporates nitrogen in the nitride films. One of the possible reaction pathways for this self-activated growth of ScN films from molecular N_2 is calculated to be energy efficient and without any energy barriers. Such a scavenging/gettering effect is not observed for the group III-A elements such as aluminum. Thus, it is not surprising that self-activated growth of binary AlN films was not observed from molecular N_2, and the film grows as FCC α-Al, the thermodynamically stable phase of Al at temperatures <660 °C.

Thermodynamically, active nitrogen has a greater affinity to bond to aluminum than to scandium. The Gibbs free energy of formation of AlN is more negative than that of ScN.[37,48] Thus, if active nitrogen species are available (either from plasma generation or from N_2 bond breaking by scandium), then Al could get nitrided, incorporated in the lattice, and it would be feasible to grow ternary Al–Sc–N nitride. Not surprisingly, we observe the self-activated growth of rock salt AlScN films for Al compositions from 0% to 47.8%, i.e., only at high Sc compositions of more than 7% to 52%. However, no nitride phase was observed for films with high Al compositions of >93%, suggesting that a nitride phase was below the detection limit or absent. This indicates that as long as large enough scandium is available to facilitate the N_2 bond breaking, Al gets nitrided and incorporated in the ternary AlScN films. However, at scandium compositions of less than 7% Sc, self-activated growth of ternary nitride films was not feasible in this study. In GaN, AlN, and AlGaN, growth is sustained mainly by plasma-generated nitrogen radicals, whereas in AlScN, Sc not only consumes these radicals but also self-catalyzes N_2 bond breaking, boosting the supply of reactive nitrogen species.[26,31] Consequently, while the AlN, GaN, and AlGaN growth rates remain unchanged with varying metal fluxes under metal-rich conditions, AlScN exhibits increased growth rates with higher Sc flux due to this catalytic effect.[31,32]

This work reports the first demonstration of self-activated growth of a ternary nitride film directly from molecular nitrogen. Aluminum is chosen as the alloying element in ScN for this study because of the extensive interest in the Al–Sc–N ternary alloy system. The wurtzite phase of AlScN has been extensively studied for its piezoelectric, high-K, ferroelectric properties, and lattice matching to wurtzite GaN;[15,17,18,23,49] while the rock salt phase of AlScN has been theoretically explored for its potential for energy-efficient, power electronic devices due to their outstanding elastic, mechanical, and thermodynamic properties above room temperature such as high Young's modulus, shear modulus, melting temperature, Debye temperature, heat capacity, and minimum heat conduction.[50] Rock salt AlScN with lattice constants of 4.50–4.06 Å for 0%–100% Al has been predicted to be lattice matched to wurtzite AlScN[38,50] as well as to multiple conducting and superconducting transition metal nitrides, such as TiN (a_{TiN} = 4.24 Å), NbN (a_{NbN} = 4.39 Å), and TaN (a_{TaN} = 4.34 Å) at ∼54%, 12%, and 25% Al, respectively.[42] Lattice-matched rock salt AlScN and TiN heterostructures, in particular, were developed for Josephson junctions and plasmonic hyperbolic metamaterials,[14] enhanced thermoelectrics,[51] and hard coating applications.[52] Al–Sc alloys represent an emerging category of high-strength, lightweight structural materials, serving as viable candidates for aerospace and automotive applications.[43] Moreover, alloying ultrawide bandgap AlN and ScN allows for bandgap engineering and tunability from the infrared regime to the UV regime within the same material system.[42] ⟨111⟩ rock salt AlScN with a lattice constant of ∼4.40 Å is expected to have an in-plane lattice parameter of 3.11 Å lattice matched to wurtzite ⟨0001⟩ AlN, opening interesting opportunities for novel heterostructures and devices.

IV. CONCLUSION

Our report of the self-activated synthesis of crystalline ternary AlScN nitride films directly from molecular N_2 bypasses the need for energetic plasma discharge to break N_2 bonds necessary in conventional inorganic synthesis of nitrides. These findings present an energy-efficient method for synthesizing ternary nitrides, which could decrease production costs and lessen environmental impact. The self-activated growth of ternary nitrides employs molecular N_2, a resource readily available in the atmosphere, thus it may be possible to remove the necessity for expensive precursors like NH_3, hydrazine, and methyl amines. This finding can be extended to the self-activated growth of other ternary nitrides formed by combining nitrides for transition metals, like Ti, Nb, Y, W, Mo, Zr, La, etc.,[53,54] that show scavenging effects and group III-A nitrides of Al, Ga, In, etc.

The ternary group-III nitride of rock salt AlScN can be grown directly from molecular N_2 without plasma. Such self-activated epitaxial growth of rock salt AlScN films is feasible at low Al and high Sc compositions, possibly because the scavenging nature of Sc facilitates N_2 bond breaking. At high Al and low Sc compositions, the self-activated growth of the ternary nitride was not feasible in this study. The lattice parameters of self-activated rock salt AlScN films decrease with increasing Al composition. The self-activated cubic rock salt AlScN films, as well as intermetallic Al_xSc and FCC α-Al phases, exhibit twinning and are epitaxial to the substrate with their $[111]/[01\bar{1}] \parallel$ 6H-SiC $[0001]/[11\bar{2}0]$. The findings open new avenues for the ultralow-energy synthesis of ternary nitrides and devices with enhanced functionalities of transition, rare-earth metal nitrides, and group III-A metal nitrides.

SUPPLEMENTARY MATERIAL

See the supplementary material for the reflection high-energy electron diffraction (RHEED) patterns of $Al_xSc_{1-x}N_y$ films with Al composition from 0% to 100%.

ACKNOWLEDGMENTS

This work was supported by SUPREME, one of seven centers in JUMP 2.0, a Semiconductor Research Corporation (SRC) program sponsored by DARPA (characterization). The authors acknowledge the use of the Cornell NanoScale Facility (CNF), a member of the National Nanotechnology Coordinated Infrastructure (NNCI), which is supported by the National Science Foundation (NSF Grant No. NNCI-2025233). This work used the Cornell Center for Materials Research (CCMR) Shared Facilities, funded through the NSF MRSEC program (No. DMR-1719875).

AUTHOR DECLARATIONS

Conflict of Interest

The authors have no conflicts to disclose.

Author Contributions

Chandrashekhar Savant: Conceptualization (lead); Data curation (lead); Formal analysis (lead); Investigation (equal); Methodology (lead); Software (equal); Validation (equal); Writing – original draft (lead); Writing – review & editing (lead). **Rishabh Singh:** Data curation (equal); Formal analysis (equal); Validation (equal); Writing – original draft (equal); Writing – review & editing (equal). **Thai-Son Nguyen:** Data curation (equal); Formal analysis (equal); Validation (equal). **Joseph Casamento:** Conceptualization (supporting); Project administration (supporting); Supervision (equal); Validation (supporting); Writing – review & editing (supporting). **Huili Grace Xing:** Funding acquisition (equal); Project administration (equal); Resources (equal); Supervision (equal). **Debdeep Jena:** Conceptualization (equal); Funding acquisition (equal); Project administration (equal); Resources (equal); Supervision (equal); Validation (equal); Writing – review & editing (equal).

DATA AVAILABILITY

The data that support the findings of this study are available from the corresponding author upon reasonable request.

REFERENCES

[1]D. Jena, R. Page, J. Casamento, P. Dang, J. Singhal, Z. Zhang, J. Wright, G. Khalsa, Y. Cho, and H. G. Xing, "The new nitrides: Layered, ferroelectric, magnetic, metallic and superconducting nitrides to boost the GaN photonics and electronics eco-system," Jpn. J. Appl. Phys. **58**, SC0801 (2019).
[2]I. Akasaki, "Nobel lecture: Fascinated journeys into blue light," Rev. Mod. Phys. **87**, 1119–1131 (2015).
[3]H. Amano, "Nobel lecture: Growth of GaN on sapphire via low-temperature deposited buffer layer and realization of *p*-type GaN by Mg doping followed by low-energy electron beam irradiation," Rev. Mod. Phys. **87**, 1133–1138 (2015).
[4]S. Nakamura, "Nobel lecture: Background story of the invention of efficient blue InGaN light emitting diodes," Rev. Mod. Phys. **87**, 1139–1151 (2015).
[5]O. Knotek, W. D. Münz, and T. Leyendecker, "Industrial deposition of binary, ternary, and quaternary nitrides of titanium, zirconium, and aluminum," J. Vac. Sci. Technol. A **5**, 2173–2179 (1987).
[6]C. Savant, V. Gund, K. Nomoto, T. Maeda, S. Jadhav, J. Lee, M. Ramesh, E. Kim, T.-S. Nguyen, Y.-H. Chen *et al.*, "Ferroelectric AlBN films by molecular beam epitaxy," Appl. Phys. Lett. **125**, 072902 (2024).
[7]C. Savant, T.-S. Nguyen, K. Nomoto, S. Vishwakarma, S. Ma, A. Dhar, Y.-H. Chen, J. Casamento, D. J. Smith, H. G. Xing *et al.*, "Epitaxial high-K barrier AlBN/GaN HEMTs," Appl. Phys. Lett. **126**, 112906 (2025).
[8]J. Hayden, M. D. Hossain, Y. Xiong, K. Ferri, W. Zhu, M. V. Imperatore, N. Giebink, S. Trolier-McKinstry, I. Dabo, and J.-P. Maria, "Ferroelectricity in boron-substituted aluminum nitride thin films," Phys. Rev. Mater. **5**, 044412 (2021).
[9]K. Kutschej, P. H. Mayrhofer, M. Kathrein, P. Polcik, R. Tessadri, and C. Mitterer, "Structure, mechanical and tribological properties of sputtered $Ti_{1-x}Al_xN$ coatings with $0.5 \leq x \leq 0.75$," Surf. Coat. Technol. **200**, 2358–2365 (2005).
[10]K. Bobzin, E. Lugscheider, R. Nickel, and P. Immich, "($Cr_{1-x}Al_x$)Nein review über ein vielseitig einsetzbares Schichtsystem," Materialwissenschaft und Werkstofftechnik: Entwicklung, Fertigung, Prüfung, Eigenschaften und Anwendungen technischer Werkstoffe **37**, 833–841 (2006).
[11]O. A. Makgae, F. Lenrick, V. Bushlya, J. M. Andersson, R. M'Saoubi, and M. Ek, "Visualising microstructural dynamics of titanium aluminium nitride coatings under variable-temperature oxidation," Appl. Surf. Sci. **618**, 156625 (2023).
[12]S. Kerdsongpanya, N. Van Nong, N. Pryds, A. Žukauskaitė, J. Jensen, J. Birch, J. Lu, L. Hultman, G. Wingqvist, and P. Eklund, "Anomalously high thermoelectric power factor in epitaxial ScN thin films," Appl. Phys. Lett. **99**, 232113 (2011).
[13]B. Saha, M. Garbrecht, J. A. Perez-Taborda, M. H. Fawey, Y. R. Koh, A. Shakouri, M. Martin-Gonzalez, L. Hultman, and T. D. Sands, "Compensation of native donor doping in ScN: Carrier concentration control and *p*-type ScN," Appl. Phys. Lett. **110**, 252104 (2017).
[14]B. Saha, G. V. Naik, S. Saber, C. Akatay, E. A. Stach, V. M. Shalaev, A. Boltasseva, and T. D. Sands, "TiN/(Al,Sc)N metal/dielectric superlattices and

multilayers as hyperbolic metamaterials in the visible spectral range," Phys. Rev. B **90**, 125420 (2014).
[15]T.-S. Nguyen, N. Pieczulewski, C. Savant, J. J. P. Cooper, J. Casamento, R. S. Goldman, D. A. Muller, H. G. Xing, and D. Jena, "Lattice-matched multiple channel AlScN/GaN heterostructures," APL Mater. **12**, 101117 (2024).
[16]A. Asteris, T.-S. Nguyen, C. F. Chang, C. Savant, P. Lonergan, H. G. Xing, and D. Jena, "High mobility multiple-channel AlScN/GaN heterostructures," arXiv:2511.10849 (2025).
[17]T. Nguyen, K. Nomoto, W. Zhao, C. Savant, H. Xing, and D. Jena, "Strain-balanced AlScN/GaN HEMTs with f_T/f_{MAX} of 173/321 GHz," in *2024 IEEE International Electron Devices Meeting (IEDM)* (IEEE, 2024), pp. 1–4.
[18]M. Akiyama, K. Kano, and A. Teshigahara, "Influence of growth temperature and scandium concentration on piezoelectric response of scandium aluminum nitride alloy thin films," Appl. Phys. Lett. **95**, 162107 (2009).
[19]S. Fichtner, N. Wolff, F. Lofink, L. Kienle, and B. Wagner, "AlScN: A III-V semiconductor based ferroelectric," J. Appl. Phys. **125**, 114103 (2019).
[20]J. Casamento, K. Nomoto, T. Nguyen, H. Lee, C. Savant, L. Li, A. Hickman, T. Maeda, J. Encomendero, V. Gund *et al.*, "FerroHEMTs: High-current and high-speed all-epitaxial AlScN/GaN ferroelectric transistors,"' in *2022 International Electron Devices Meeting (IEDM)* (IEEE, 2022), pp. 11.1.1–11.1.4.
[21]J. Casamento, T.-S. Nguyen, Y. Cho, C. Savant, T. Vasen, S. Afroz, D. Hannan, H. G. Xing, and D. Jena, "Transport properties of polarization-induced 2D electron gases in epitaxial AlScN/GaN heterojunctions," Appl. Phys. Lett. **121**, 192101 (2022).
[22]J. Casamento, H. Lee, T. Maeda, V. Gund, K. Nomoto, L. van Deurzen, W. Turner, P. Fay, S. Mu, C. G. Van de Walle *et al.*, "Epitaxial $Sc_xAl_{1-x}N$ on GaN exhibits attractive high-K dielectric properties," Appl. Phys. Lett. **120**, 152901 (2022).
[23]J. Casamento, K. Nomoto, T.-S. Nguyen, H. Lee, C. Savant, L. Li, A. Hickman, T. Maeda, Y.-T. Shao, J. Encomendero *et al.*, "AlScN high electron mobility transistors: Integrating High Piezoelectric, High K Dielectric, and Ferroelectric Functionality," in *2023 IEEE BiCMOS and Compound Semiconductor Integrated Circuits and Technology Symposium (BCICTS)* (IEEE, 2023), pp. 132–136.
[24]M. Gremmel, C. Prakash Savant, D. Bhattacharya, G. Schönweger, D. Jena, and S. Fichtner, "The effect of boron incorporation on leakage and wake-up in ferroelectric $Al_{1-x}Sc_xN$," J. Appl. Phys. **137**, 244101 (2025).
[25]R. Kalescky, E. Kraka, and D. Cremer, "Identification of the strongest bonds in chemistry," J. Phys. Chem. A **117**, 8981–8995 (2013).
[26]C. P. Savant, A. Verma, T.-S. Nguyen, L. van Deurzen, Y.-H. Chen, Z. He, S. S. Rezaie, J. Gollwitzer, B. Gregory, S. Sarker *et al.*, "Self-activated epitaxial growth of ScN films from molecular nitrogen at low temperatures," APL Mater. **12**, 111108 (2024).
[27]W. Lengauer, "Investigations in the scandium-nitrogen system," J. Solid State Chem. **76**, 412–415 (1988).
[28]R. Niewa, D. A. Zherebtsov, M. Kirchner, M. Schmidt, and W. Schnelle, "New ways to high-quality bulk scandium nitride," Chem. Mater. **16**, 5445–5451 (2004).
[29]Y. Gong, Y. Zhao, and M. Zhou, "Formation and characterization of the tetranuclear scandium nitride: Sc_4N_4," J. Phys. Chem. A **111**, 6204–6207 (2007).
[30]H. C. L. Tsui, L. E. Goff, N. P. Barradas, E. Alves, S. Pereira, H. E. Beere, I. Farrer, C. A. Nicoll, D. A. Ritchie, and M. A. Moram, "The effect of metal-rich growth conditions on the microstructure of $Sc_xGa_{1-x}N$ films grown using molecular beam epitaxy," Phys. Status Solidi A **212**, 2837–2842 (2015).
[31]K. Frei, R. Trejo-Hernández, S. Schütt, L. Kirste, M. Prescher, R. Aidam, S. Müller, P. Waltereit, O. Ambacher, and M. Fiederle, "Investigation of growth parameters for ScAlN-barrier HEMT structures by plasma-assisted MBE," Jpn. J. Appl. Phys. **58**, SC1045 (2019).
[32]Z. Engel, K. Motoki, C. M. Matthews, and W. A. Doolittle, "Overcoming metal-rich surface chemistry limitations of ScAlN for high electrical performance heterostructures," J. Appl. Phys. **132**, 185302 (2022).
[33]B. Heying, R. Averbeck, L. Chen, E. Haus, H. Riechert, and J. Speck, "Control of GaN surface morphologies using plasma-assisted molecular beam epitaxy," J. Appl. Phys. **88**, 1855–1860 (2000).
[34]C. Savant, T.-S. Nguyen, S. Vishwakarma, J. Lee, A. Ithepalli, Y.-H. Chen, K. Nomoto, F. Rana, D. J. Smith, H. G. Xing *et al.*, "Epitaxial AlBN/β-Nb_2N ferroelectric/Superconductor heterostructures," Phys. Status Solidi RRL **18**, 2400157 (2024).
[35]A. C. Thompson D. Vaughan *et al.*, *X-ray Data Booklet* (Lawrence Berkeley National Laboratory, University of California, Berkeley, CA, 2001), Vol. 8.
[36]M. J. Winiarski and D. A. Kowalska, "Crystal structure of rare earth and group III nitride alloys by ab initio calculations," Sci. Rep. **10**, 16414 (2020).
[37]K. Hirata, K. Shobu, H. Yamada, M. Uehara, S. A. Anggraini, and M. Akiyama, "Thermodynamic assessment of the Al–Sc–N ternary system and phase-separated region of the strained wurtzite phase," J. Eur. Ceram. Soc. **40**, 5410–5422 (2020).
[38]S. Satoh, K. Ohtaka, T. Shimatsu, and S. Tanaka, "Crystal structure deformation and phase transition of AlScN thin films in whole Sc concentration range," J. Appl. Phys. **132**, 025103 (2022).
[39]Y.-J. Liao, C.-W. Cheng, B.-H. Wu, C.-Y. Wang, C.-Y. Chen, S. Gwo, and L.-J. Chen, "Low threshold room-temperature UV surface plasmon polariton lasers with ZnO nanowires on single-crystal aluminum films with Al_2O_3 interlayers," RSC Adv. **9**, 13600–13607 (2019).
[40]J. Casamento, J. Wright, R. Chaudhuri, H. G. Xing, and D. Jena, "Molecular beam epitaxial growth of scandium nitride on hexagonal SiC, GaN, and AlN," Appl. Phys. Lett. **115**, 172101 (2019).
[41]M. Henini, *Molecular Beam Epitaxy: From Research to Mass Production* (Elsevier, 2012).
[42]J. M. Waack, M. Kremer, M. Czerner, and C. Heiliger, "Structural and electronic properties of cubic rocksalt $Al_xSc_{1-x}N$ random alloys from ab initio calculations," Phys. Rev. B **109**, 075142 (2024).
[43]A. Gupta, B. Tas, D. Korbmacher, B. Dutta, Y. Neitzel, B. Grabowski, T. Hickel, V. Esin, S. V. Divinski, G. Wilde *et al.*, "A combined experimental and first-principles based assessment of finite-temperature thermodynamic properties of intermetallic Al_3Sc," Materials **14**, 1837 (2021).
[44]M. J. Winiarski and D. Kowalska, "Electronic structure of REN (RE= Sc, Y, La, and Lu) semiconductors by MBJLDA calculations," Mater. Res. Express **6**, 095910 (2019).
[45]B. Saha, J. Acharya, T. D. Sands, and U. V. Waghmare, "Electronic structure, phonons, and thermal properties of ScN, ZrN, and HfN: A first-principles study," J. Appl. Phys. **107**, 033715 (2010).
[46]S. Acharya, A. Chatterjee, V. Bhatia, A. I. K. Pillai, M. Garbrecht, and B. Saha, "Twinned growth of ScN thin films on lattice-matched GaN substrates," Mater. Res. Bull. **143**, 111443 (2021).
[47]W. Witt, "Absolute präzisionsbestimmung von gitterkonstanten an germanium-und aluminium-einkristallen mit elektroneninterferenzen," Zeitschrift für Naturforschung A **22**, 92–95 (1967).
[48]W. E. Hoke, A. Torabi, J. J. Mosca, and T. D. Kennedy, "Thermodynamic analysis of cation incorporation during molecular beam epitaxy of nitride films using metal-rich growth conditions," J. Vac. Sci. Technol. B **25**, 978–982 (2007).
[49]T.-S. Nguyen, C. Savant, A. Asteris, H. G. Xing, and D. Jena, "Transport properties of lattice-matched AlScN/GaN single-and multichannel heterostructures," Appl. Phys. Lett. **127**, 102106 (2025).
[50]O. Ambacher, S. Mihalic, M. Yassine, A. Yassine, N. Afshar, and B. Christian, "Structural, elastic, and thermodynamic properties of cubic and hexagonal $Sc_xAl_{1-x}N$ crystals," J. Appl. Phys. **134**, 160702 (2023).
[51]J. L. Schroeder, B. Saha, M. Garbrecht, N. Schell, T. D. Sands, and J. Birch, "Thermal stability of epitaxial cubic-TiN/(Al, Sc) N metal/semiconductor superlattices," J. Mater. Sci. **50**, 3200–3206 (2015).
[52]B. Saha, S. K. Lawrence, J. L. Schroeder, J. Birch, D. F. Bahr, and T. D. Sands, "Enhanced hardness in epitaxial TiAlScN alloy thin films and rocksalt TiN/(Al, Sc)N superlattices," Appl. Phys. Lett. **105**, 151904 (2014).
[53]A. Gupta and J. Leck, "An evaluation of the titanium sublimation pump," Vacuum **25**, 362–372 (1975).
[54]J. Haygood, D. Trayer, and R. Brown, "Review on the vacuum pumping of hydrogen," Arnold Engineering Development Center TR-69-109, Arnold Air Force Station, Tullahoma, TN, 1969.